Supplemetary Information

$MnFe_2O_4$-Decorated Large-Pore Mesoporous Silica Coated Upconversion Nanoparticles for Near-Infrared Light Induced and O_2 Self-Sufficient Photodynamic Therapy

Binbin Ding,[†a,b] Shuai Shao,[†a,c] Haihua Xiao,[d] Chunqiang Sun,[a] Xuechao Cai,[a] Fan Jiang,[a,b] Xueyan Zhao,[a] Ping'an Ma*[a,b] and Jun Lin*[a,b,e]

[a] *State Key Laboratory of Rare Earth Resource Utilization, Changchun Institute of Applied Chemistry, Chinese Academy of Sciences, Changchun 130022, P. R. China*

[b] *University of Science and Technology of China, Hefei 230026, P. R. China*

[c] *Changchun University of Science and Technology, Changchun 130022, P. R. China*

[d] *State Key Laboratory of Polymer Physics and Chemistry, Beijing National Laboratory for Molecular Sciences, Institute of Chemistry, Chinese Academy of Sciences, Beijing 100190, P. R. China*

[e] *School of Applied Physics and Materials, Wuyi University, Jiangmen, Guangdong 529020, P. R. China*

† Binbin Ding and Shuai Shao contributed equally.

** Corresponding author. E-mail: jlin@ciac.ac.cn (Prof. Jun Lin) and mapa675@ciac.ac.cn (Dr. Ping'an Ma)*

Cell lines and animals

L929 (mouse fibroblast cell line) and HepG2 cells (human liver cancer line) were chosen for cell tests. L929 and HepG2 cells were purchased from the Institute of Biochemistry and Cell Biology, Chinese Academy of Sciences. L929 cells were first cultured in Dulbecco's Modified Eagle's Medium (DMEM) supplemented with 10% heat-inactivated fetal bovine serum (FBS, GIBCO), 100 units per mL of penicillin and 100 units per mL of streptomycin (Sigma) in an atmosphere of 5% CO_2 at 37 °C. HepG2 cells were first cultured in DMEM supplemented with 10% heat-inactivated FBS, 100 units per mL of penicillin and 100 units per mL of streptomycin in an atmosphere of 5% CO_2 at 37 °C. Female nude mice and Balb/c mice (19-22 g) were purchased from the Center for Experimental Animals, Beijing Vital River Laboratory Animal Technology Co, Ltd. All mice were handled using the protocol approved by the Institutional Animal Care and Use Committee of Jilin University.

Material Characterization

The transmission electron microscopy (TEM) and high resolution transmission electron microscopy (HRTEM) images of samples were obtained using a FEI Tecnai G2 S-Twin with a field emission gun operating at 200 kV. Their crystal structure was determined by X-ray powder diffraction (Bruker) equipped with Cu-Kα radiation (λ=0.154 nm). Nitrogen adsorption/desorption analysis was measured with a Micromeritics ASAP 2020M apparatus. The UC-emission spectra were collected on HitachiF-7000 spectrophotometer excited with the 980 nm CW laser from an optical parametric oscillator (Continuum Sunlite, USA) as the excitation source and detected

by an R955 (Hamamatsu) from 300 to 700 nm. The UV-vis absorption spectra were obtained from U-3100 spectrophotometer (Hitachi). The X-ray photoelectron spectra (XPS) were taken on a VG ESCALAB MK II electron spectrometer using Mg Kα (1200 eV) as the excitation source, putting the samples on silicon slice. Magnetic resonance imaging (MRI) was recorded on a 1.2 T MRI magnet (Shanghai Niumai Corporation Ration NM120-Analyst). UCL imaging was recorded on an in vivo Maestro whole-body imaging system equipped with an external 980 nm laser as the excitation source.

Histological analysis

For haematoxylin and eosin (H&E) staining, heart, liver, spleen, lung and kidney were harvested, fixed in 10% neutral buffered formalin, processed routinely into paraffin, sectioned into thin slices, and stained with H&E for histological analysis. Analysis of Variance (ANOVA) was used to assess statistical significance. $^{*}p<0.05$, $^{**}p< 0.01$, $^{***}p<0.001$.

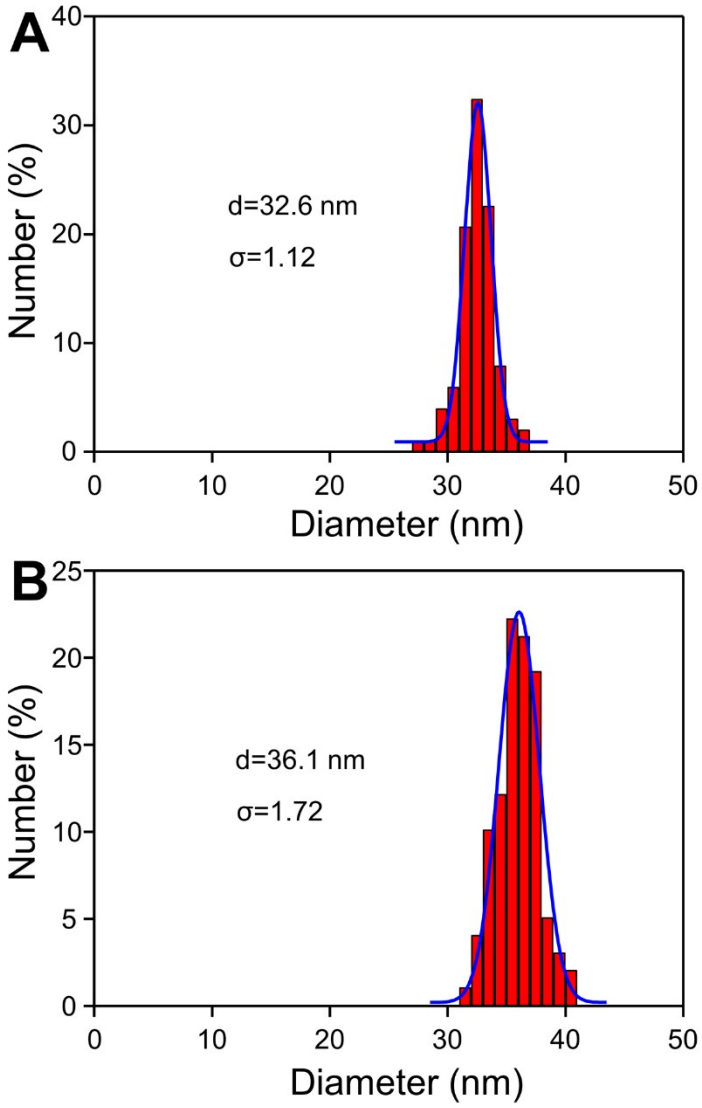

Figure S1. The size distributions of β-$NaYF_4$:20%Yb,2%Er (A. d=32.6 nm, σ=1.12) and β-$NaYF_4$:20%Yb,2%Er @$NaYF_4$ (B. d=36.1 nm, σ=1.72). The change of sizes of nanoparticles suggested that the inert shell was successfully coated onto the core to form β-$NaYF_4$:20%Yb,2%Er @$NaYF_4$ core-shell UCNPs.

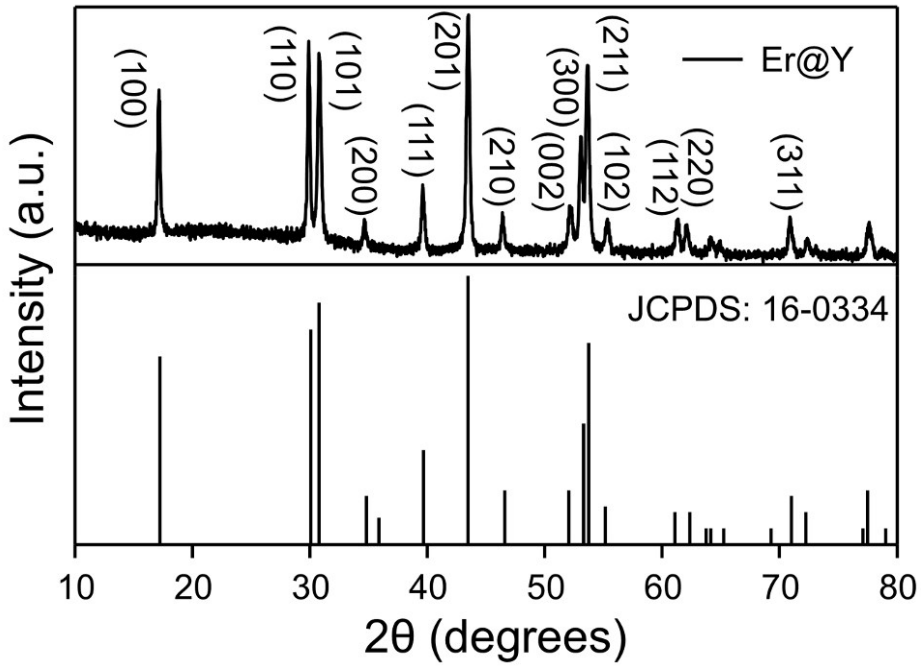

Figure S2. X-ray diffraction (XRD) pattern of β-$NaYF_4$:20%Yb,2%Er@β-$NaYF_4$ core-shell UCNPs, which could be well indexed to the β-$NaYF_4$ (JCPDS No. 16-0334).

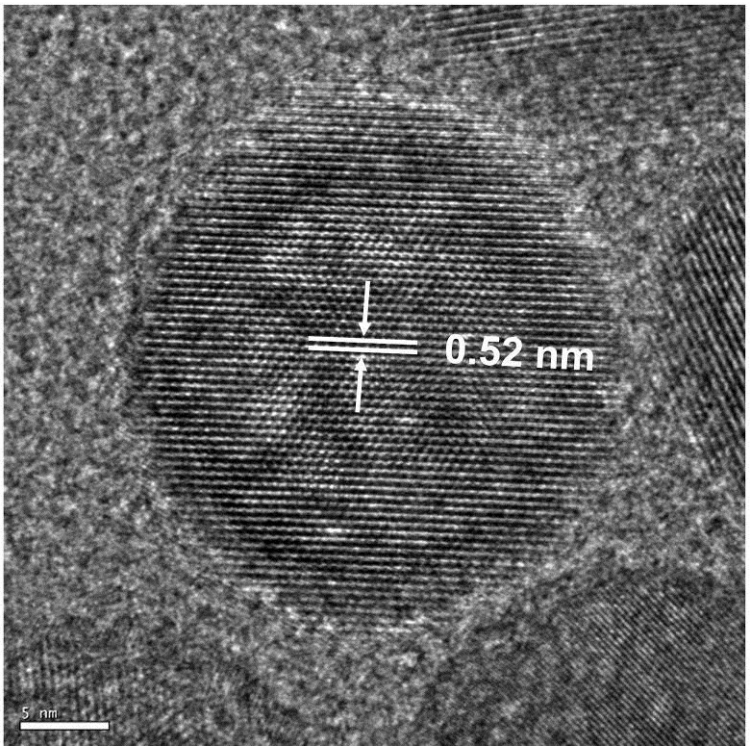

Figure S3. The high-resolution TEM (HRTEM) of β-$NaYF_4$:20%Yb,2%Er. The lattice distance in β-$NaYF_4$:20%Yb,2%Er measured from HRTEM was 0.52 nm, which can be indexed to (100) or (010) plane.

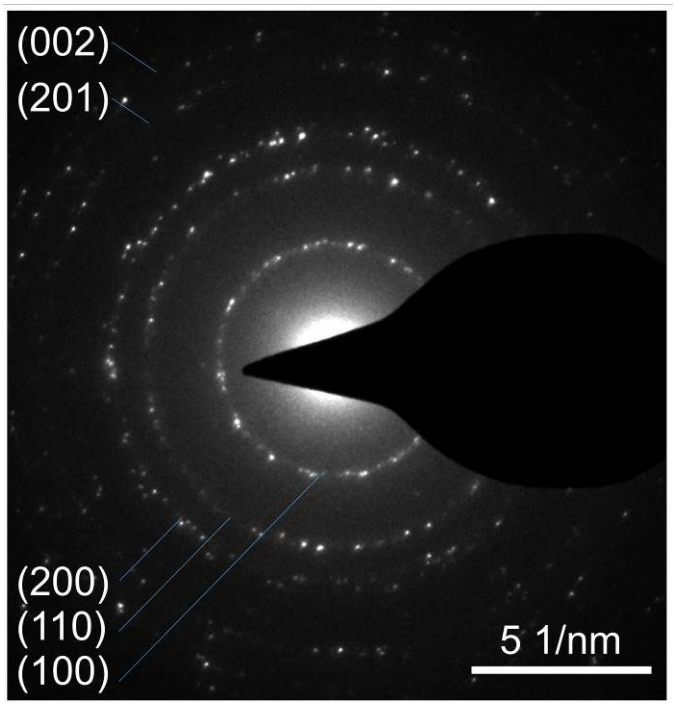

Figure S4. The diffraction spots/rings can be indexed as (100), (110), (200), (201) and (002) reflections according to the structure of *β*-$NaYF_4$:20%Yb,2%Er. The appearance of diffraction rings/spots indicates that the prepared *β*-$NaYF_4$:20%Yb,2%Er core UCNPs are composed of polycrystalline domains.

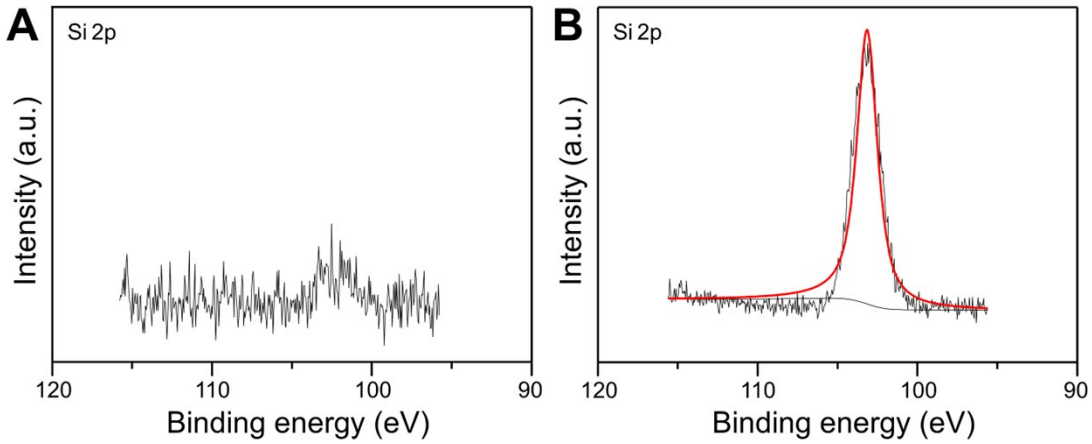

Figure S5. X-ray photoelectron spectroscopy (XPS) high-resolution scans of Si2p peaks in UCNPs (A) and UCMSs (B).

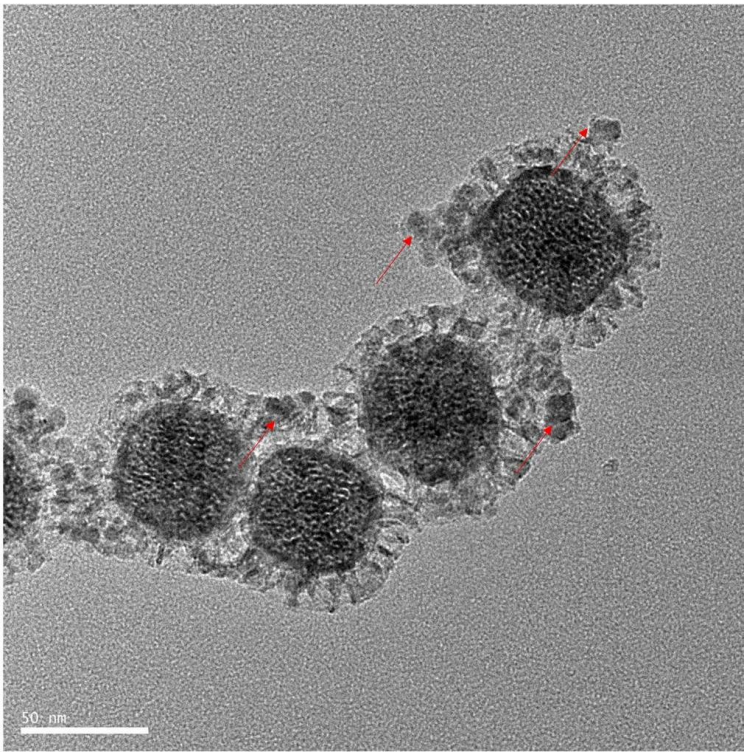

Figure S6. TEM images of UCMnFe (the $MnFe_2O_4$ to UCMSs ratio is 1:1), indicating that $MnFe_2O_4$ (red arrow) attached to the UCMSs successfully.

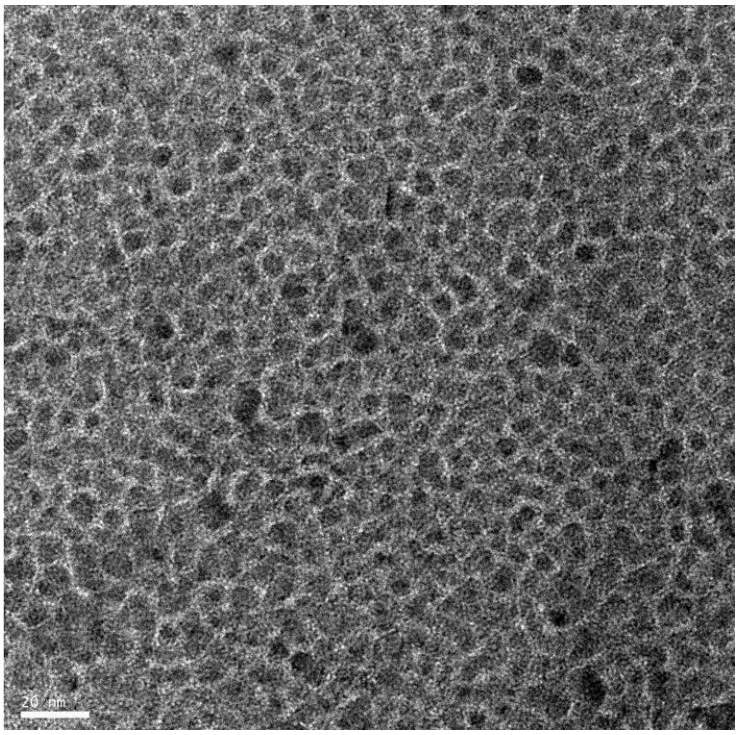

Figure S7. TEM image of $MnFe_2O_4$.

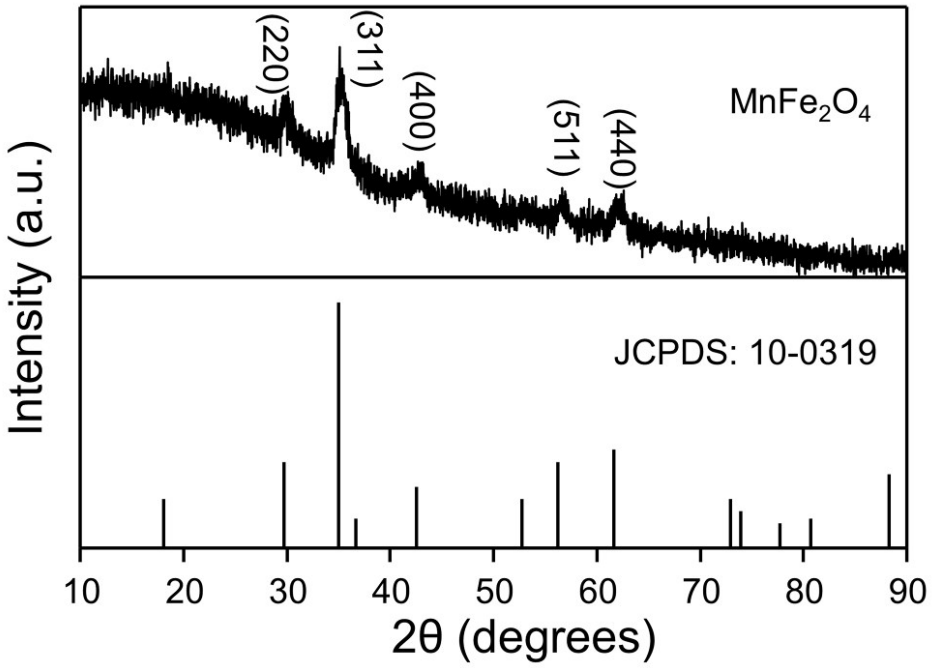

Figure S8. The XRD pattern of the prepared $MnFe_2O_4$, which could be well indexed to the $MnFe_2O_4$ (JCPDS No. 10-0319).

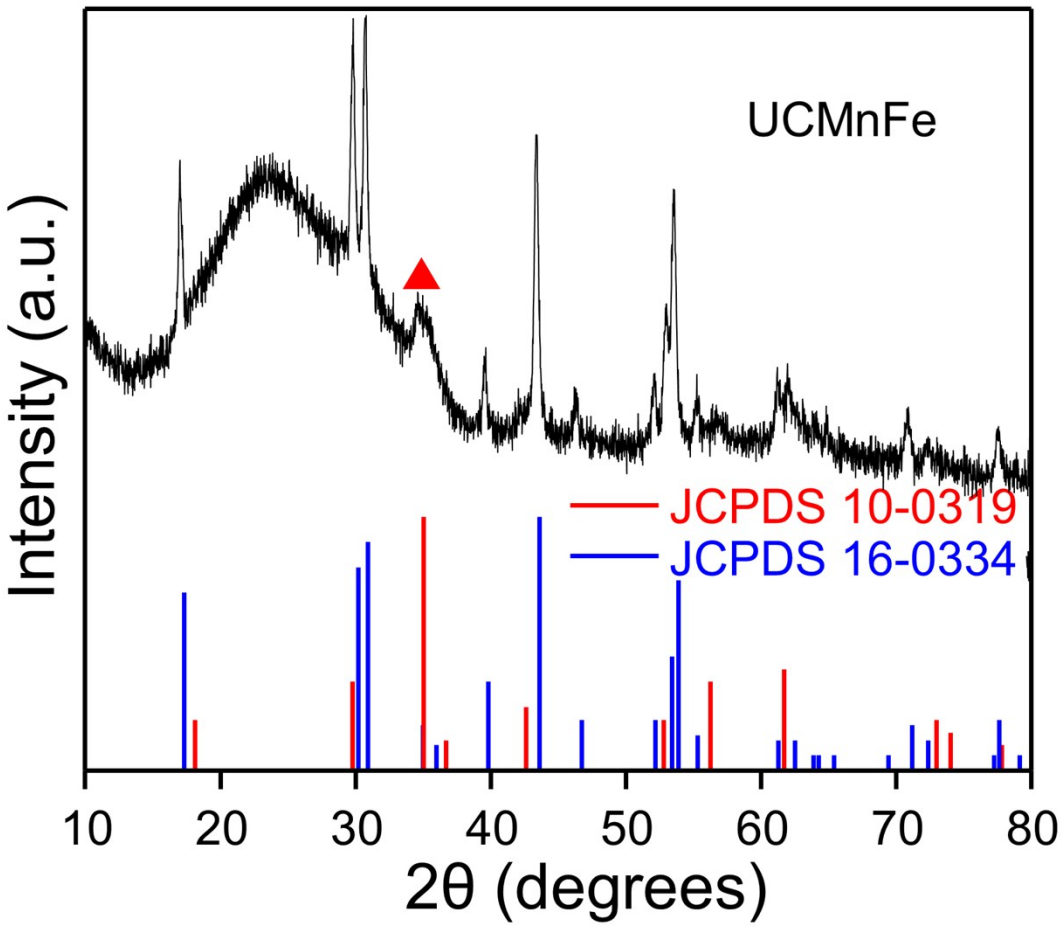

Figure S9. The XRD pattern of the prepared UCMnFe, which could be well indexed to the β-$NaYF_4$ (JCPDS No. 16-0334) and $MnFe_2O_4$ (JCPDS No. 10-0319).

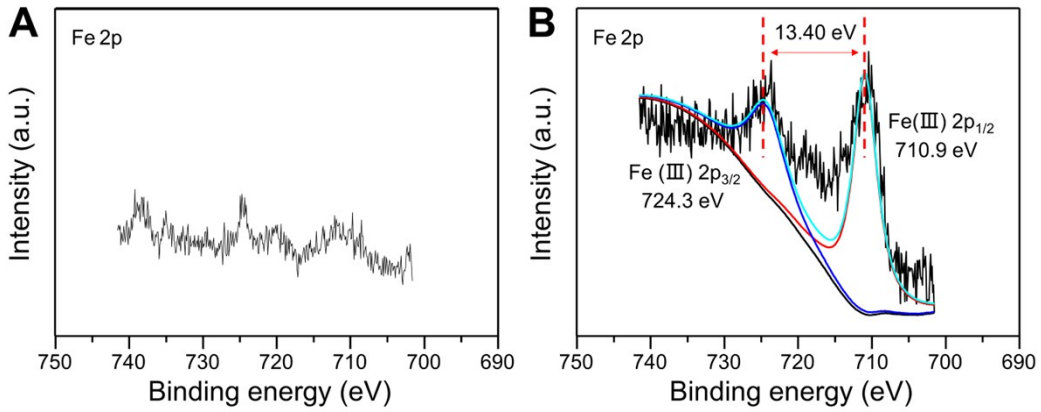

Figure S10. XPS high-resolution scans of Fe2p peaks in UCMSs (A) and UCMnFe (B).

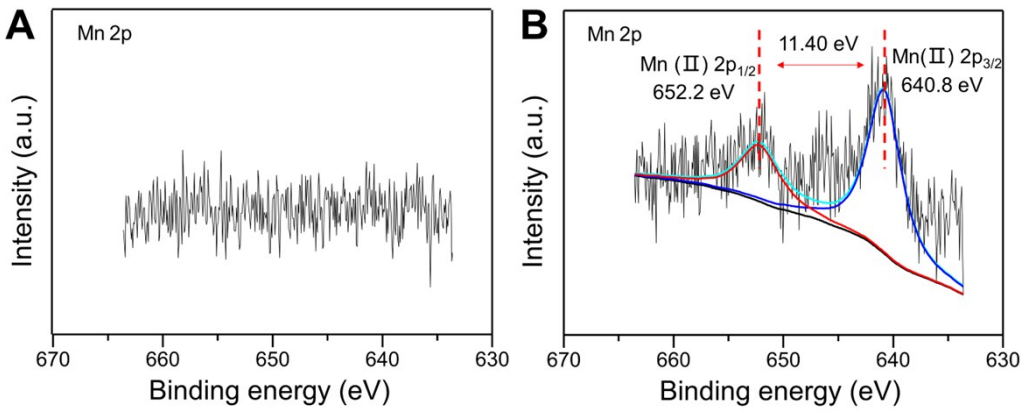

Figure S11. XPS high-resolution scans of Mn2p peaks in UCMSs (A) and UCMnFe (B).

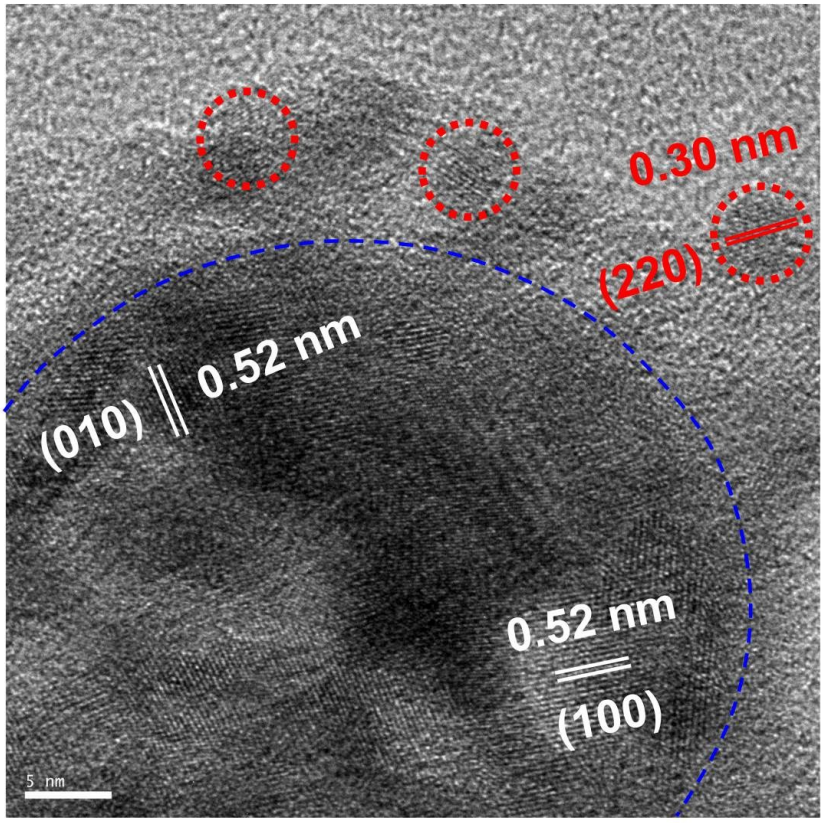

Figure S12. The high-resolution transmission electron microscopy (HRTEM) of UCMnFe (1:1). The lattice distance in UCNPs measured from HRTEM is 0.52 nm, which can be indexed to (100) or (010) plane. And the lattice distance in $MnFe_2O_4$ measured from HRTEM is 0.30 nm, which can be indexed to (220) plane.

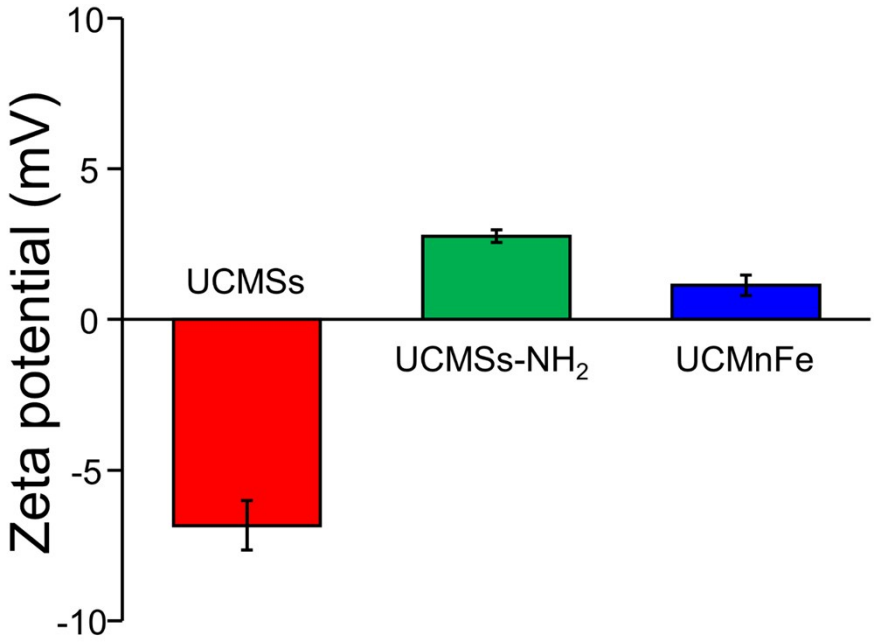

Figure S13. Zeta potentials of UCMSs, UCMSs-NH_2, UCMnFe detected by dynamic light scattering (DLS).

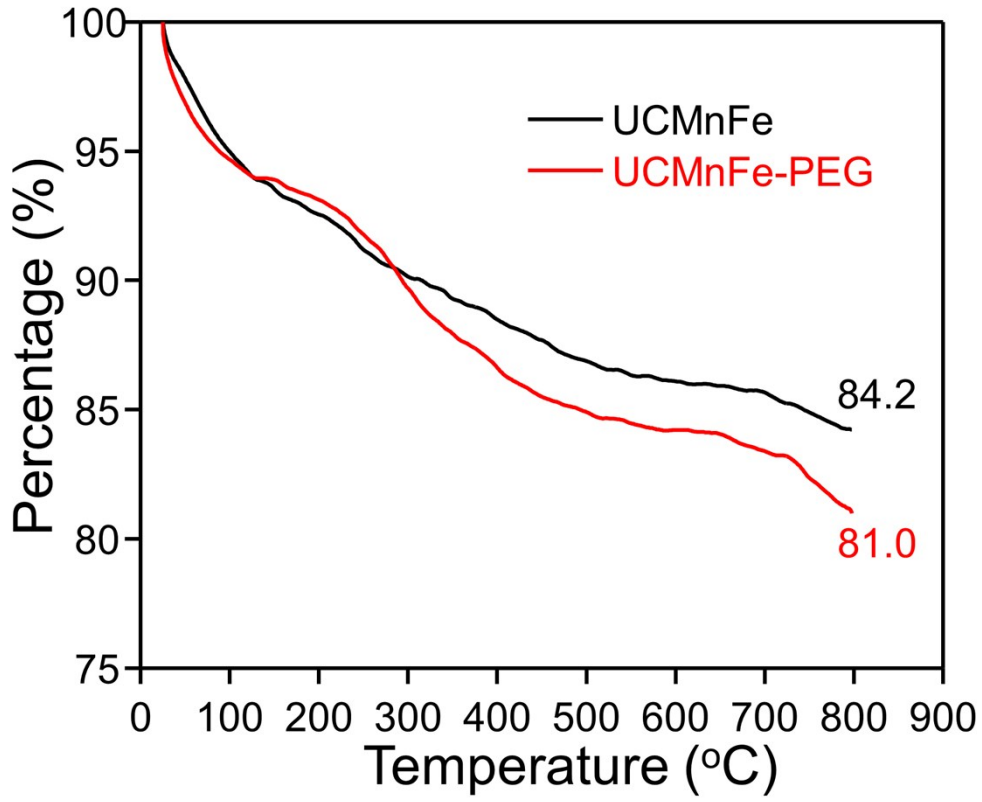

Figure S14. Thermogravimetric analysis (TGA) of a dried sample of UCMnFe and UCMnFe-PEG in the temperature range from room temperature to 800 °C at a heating rate of 10 °C/min in nitrogen.

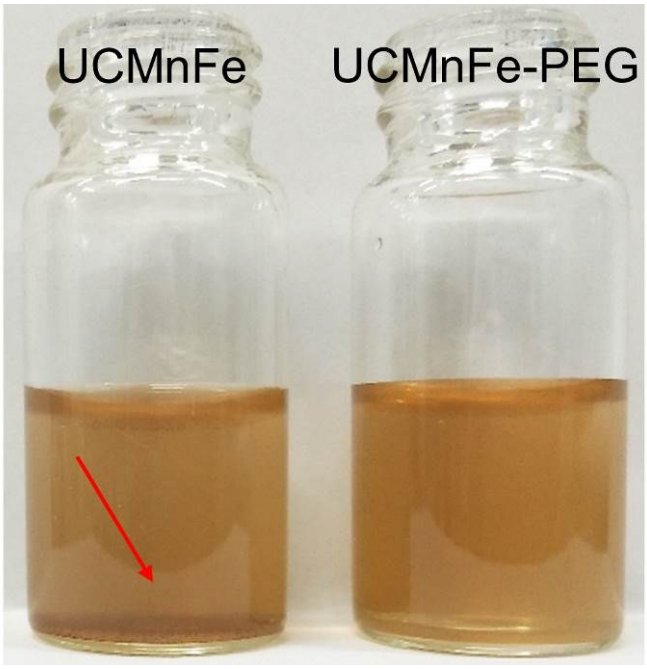

Figure S15. Digital photographs for the dispersion status of UCMnFe and UCMnFe-PEG.

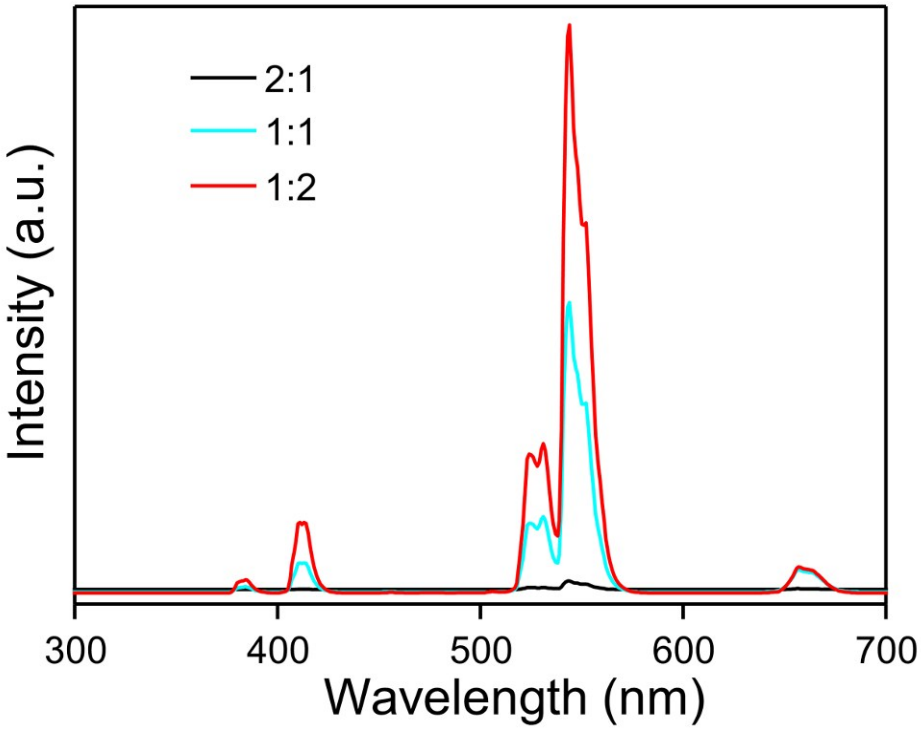

Figure S16. The upconversion emission spectra of UCMnFe with different $MnFe_2O_4$ attached to the UCMSs under 980 nm laser excitation. The $MnFe_2O_4$ to UCMSs ratio is 1:2 (red line), 1:1 (sapphire line) and 2:1 (black line), respectively.

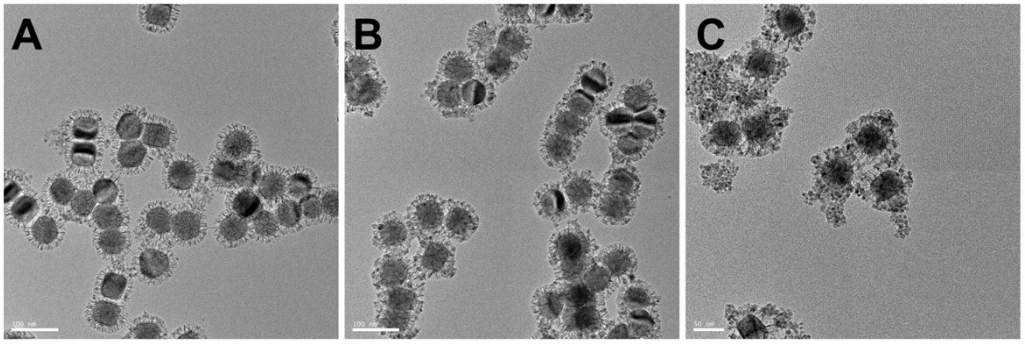

Figure S17. TEM images of UCMnFe with different $MnFe_2O_4$ attached to the UCMSs. The $MnFe_2O_4$ to UCMSs ratio is 1:2 (A), 1:1 (B) and 2:1 (C), respectively.

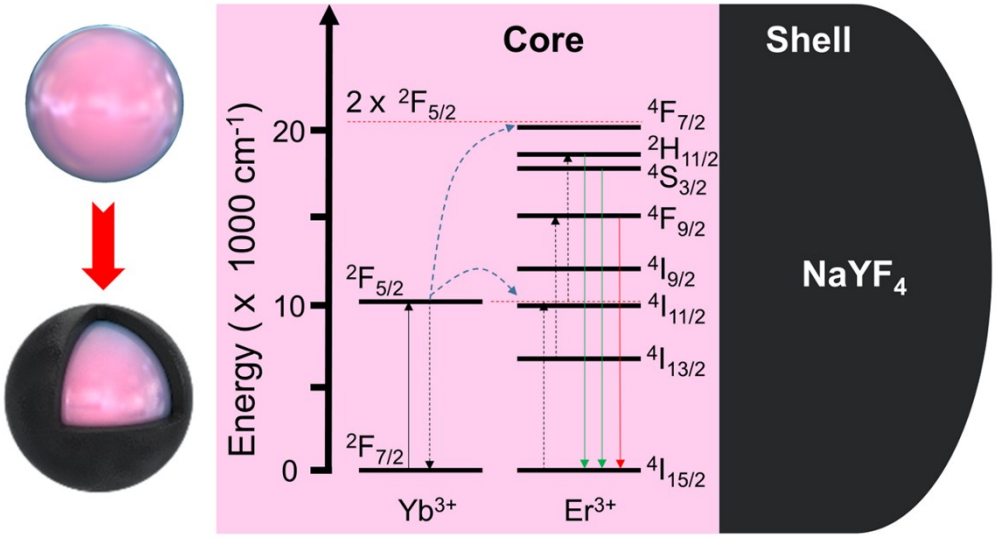

Figure S18. The proposed energy transfer mechanism under 980 nm NIR laser irradiation in β-$NaYF_4$:20%Yb,2%Er@β-$NaYF_4$ core-shell UCNPs.

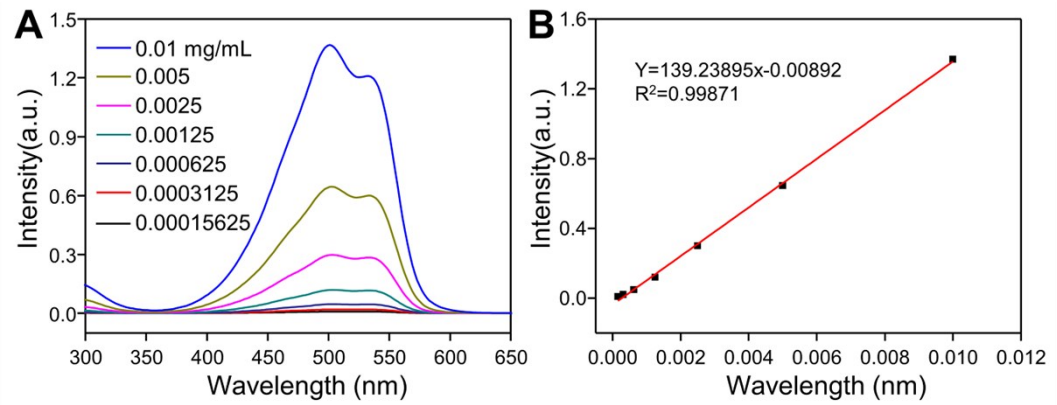

Figure S19. Determination of the amount of MC540 on the UCMSs particle. (A) The absorption spectra of MC540 with different concentrations (0.01, 0.005, 0.0025, 0.00125, 0.000625, 0.0003125 and 0.00015625 mg/mL). (B) Plot of the MC540 calibration dataset showing the change in absorption intensity of MC540 as a function of concentration. The absorption intensity was measured at 500 nm.

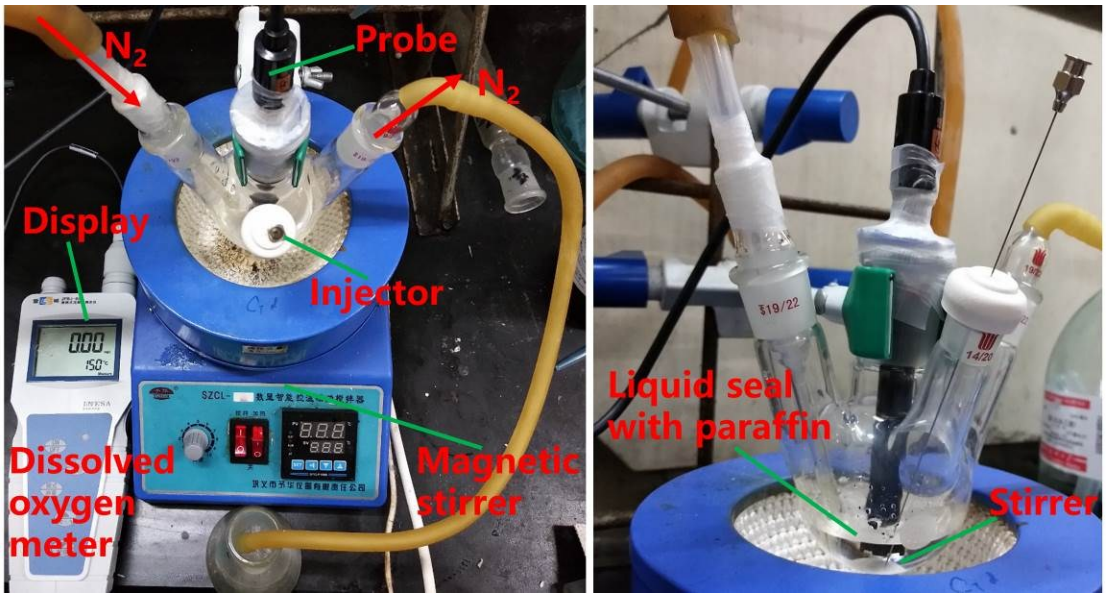

Figure S20. A dissolved oxygen meter (JPBJ-608, INESA, China) was used to measure the concentration of oxygen.

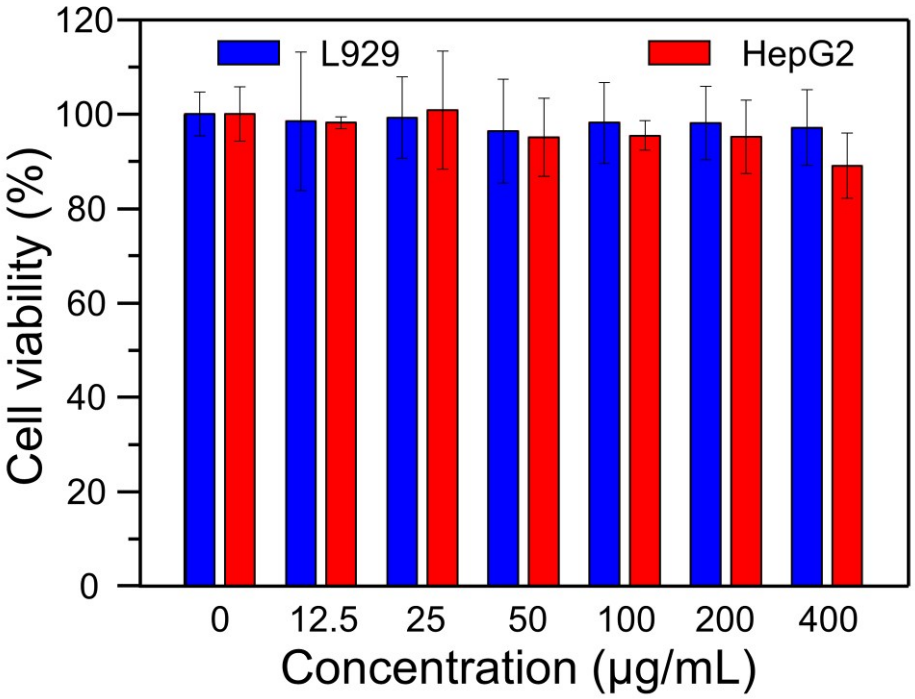

Figure S21. MTT assay of relative cell viability of L929 and HepG2 cells incubated with different concentrations (0, 12.5, 25, 50, 100, 200 and 400 μg mL^{-1}) of UCMnFe for 24 h.

Figure S22. Hypoxia incubator chamber.

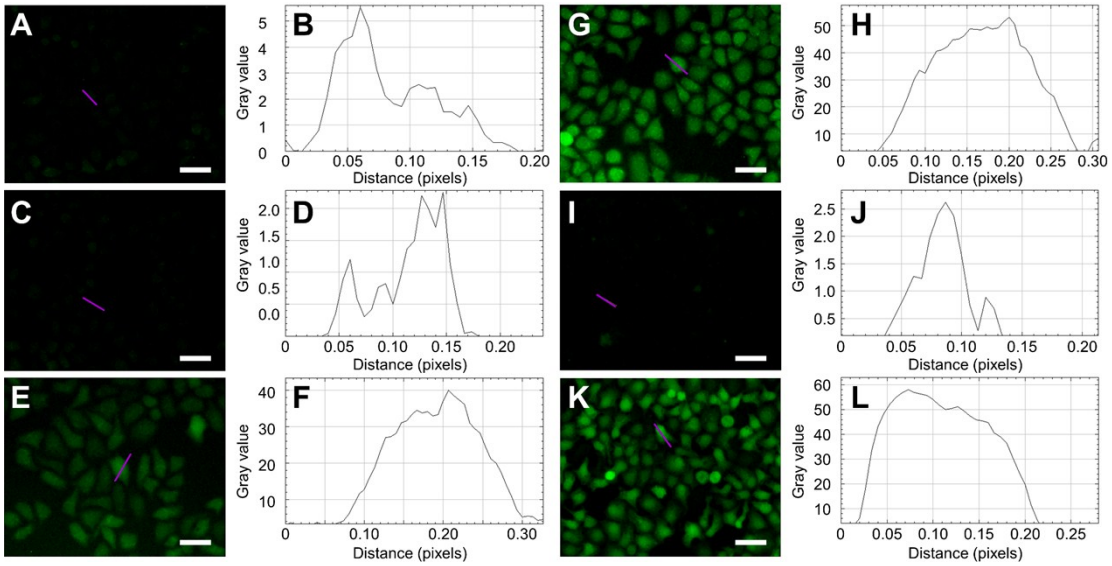

Figure S23. Intracellular ROS production with different treatments using DCFH-DA as a probe. (A-B) UCMSs-PS (-), (C-D) UCMnFe-PS (-), (E-F) UCMSs-PS (+) and (G-H) UCMnFe-PS (+) under normoxic condition. (I-J) UCMSs-PS (+) and (K-L) UCMnFe-PS (+) under hypoxia condition. Hypoxic condition was obtained via incubating the cells under a hypoxic atmosphere (1% O_2, 5% CO_2, and 94% N_2) for 24 hours using a hypoxia incubator chamber. All scale bars are 10 μm. The relative intensity of DCF was determined using linear scans to obtain quantitative data (Image J).

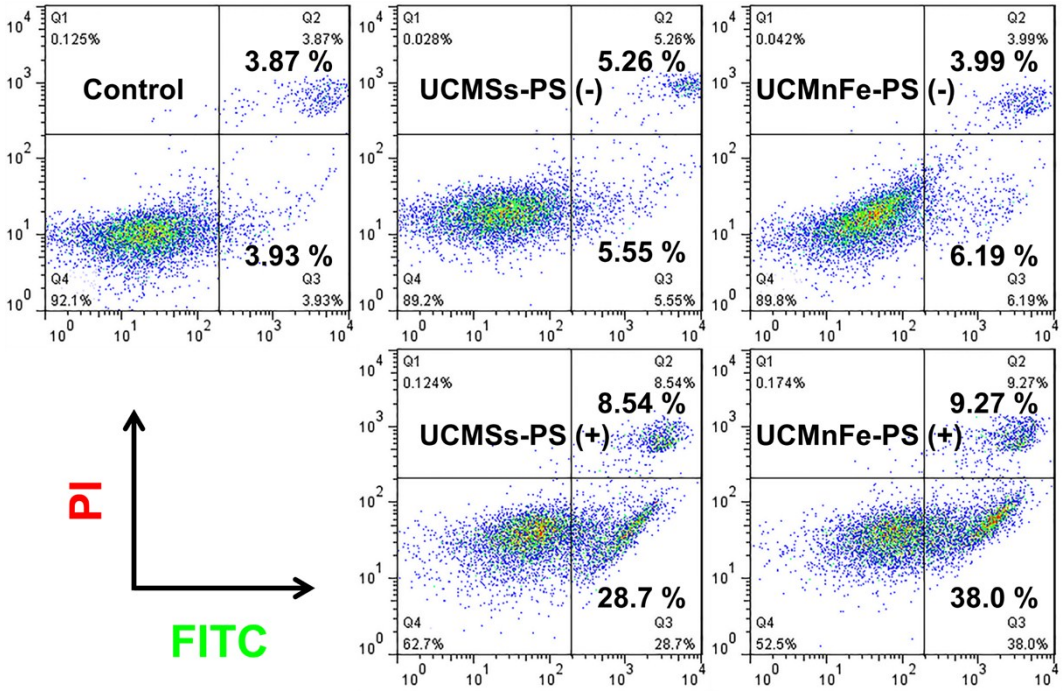

Figure S24. Flow-cytometry apoptosis assay of HepG2 cells after incubation with UCMSs-PS or UCMnFe-PS under different treatments followed by staining with Annexin-FITC and PI.

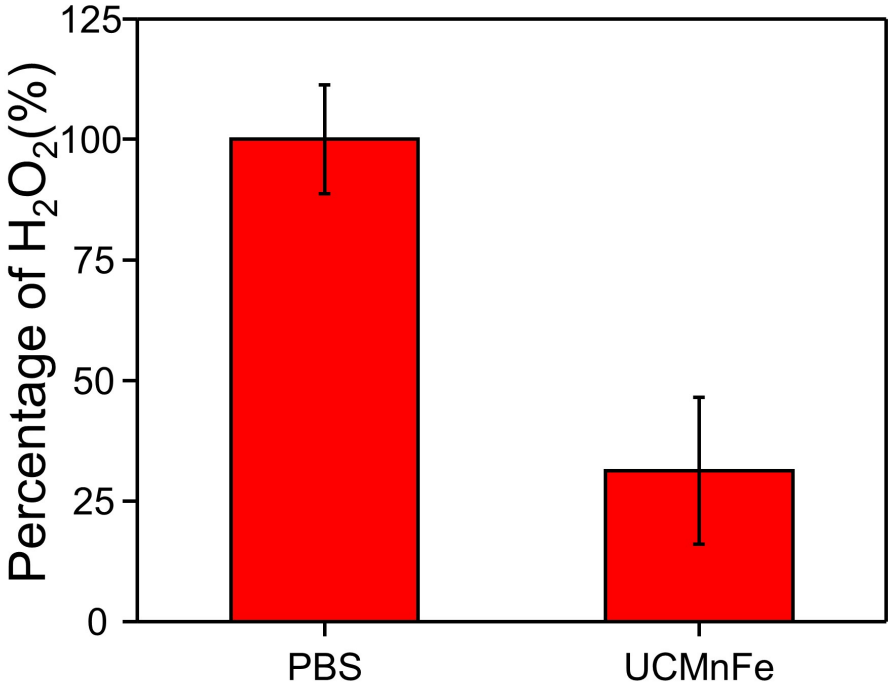

Figure S25. Intracellular H_2O_2 detections of HepG2 cells with different treatments.

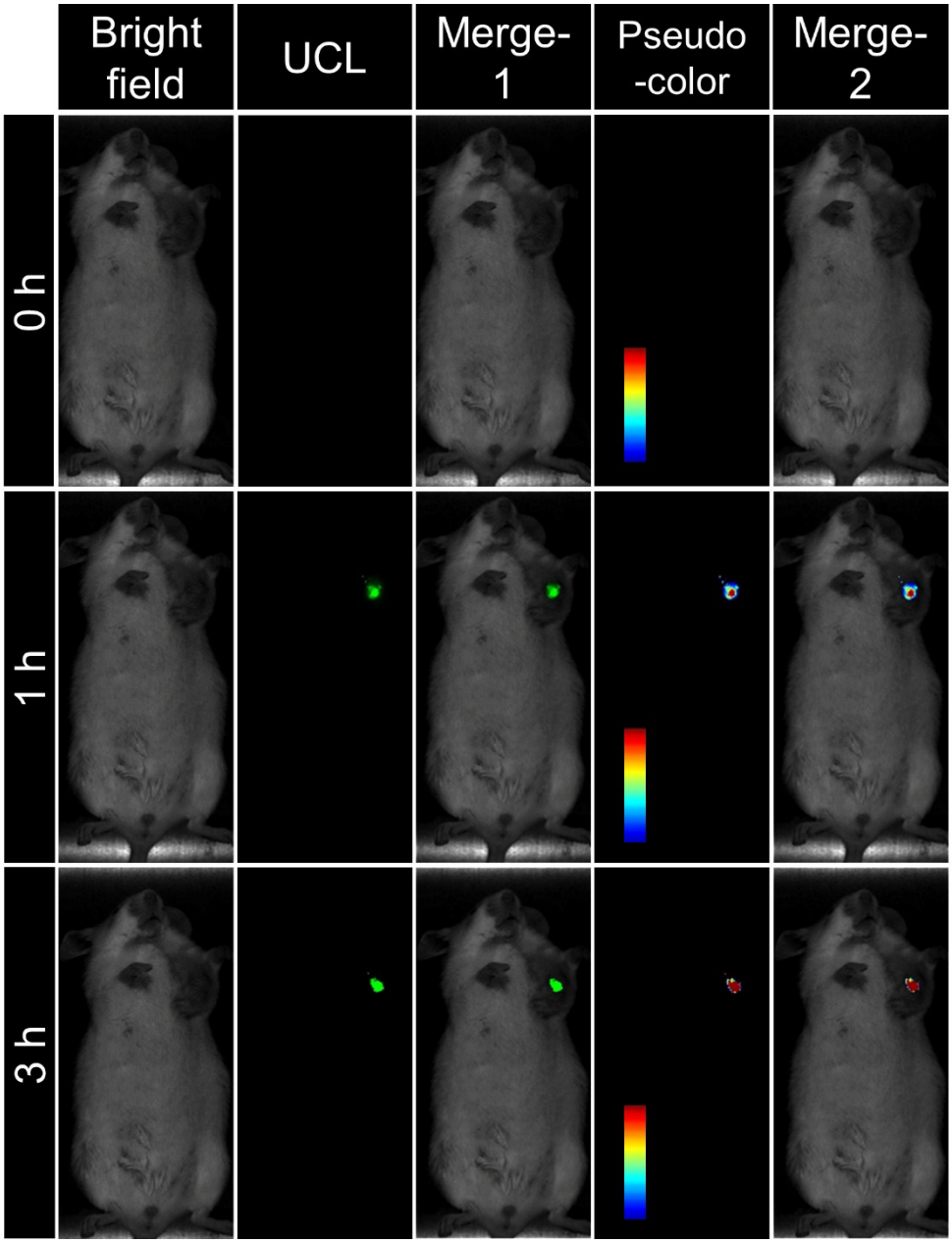

Figure S26. UCL images of a tumor-bearing mouse with tail vein injection of UCMnFe-PEG solution. The mouse was imaged on an in vivo Maestro whole-body imaging system equipped with an external 980 nm laser as the excitation source at various time periods (0 h, 1 h and 3 h). Each series can be classified into bright field, UCL, merge-1 of both above, pseudo-color and merge-2 of pseudo-color and bright field, respectively.

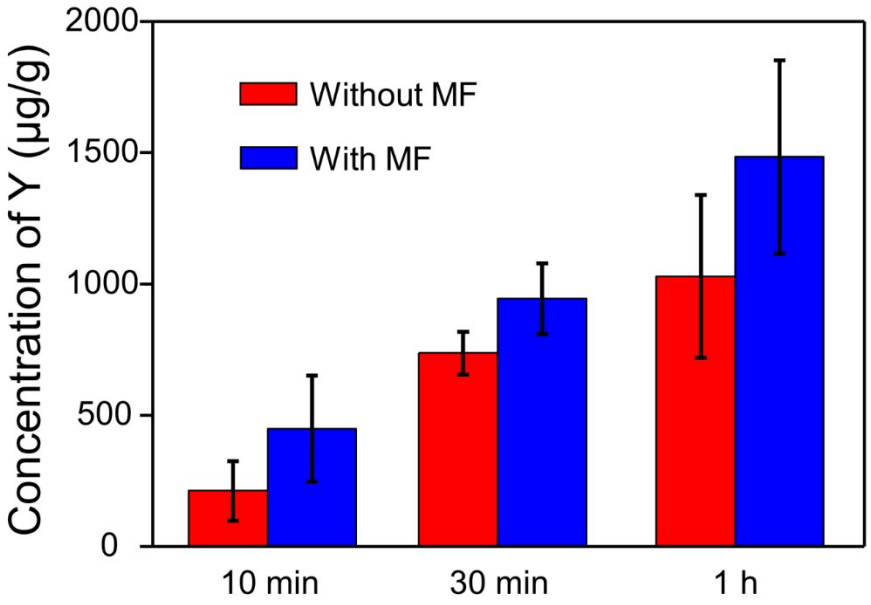

Figure S27. Magnetically targeted accumulation of UCMnFe in mice with tail vein injection of UCMnFe-PEG solution without or with magnetic guidance was determined by Y concentrations using ICP-AES for different time points (10 min, 30 min and 1 h).

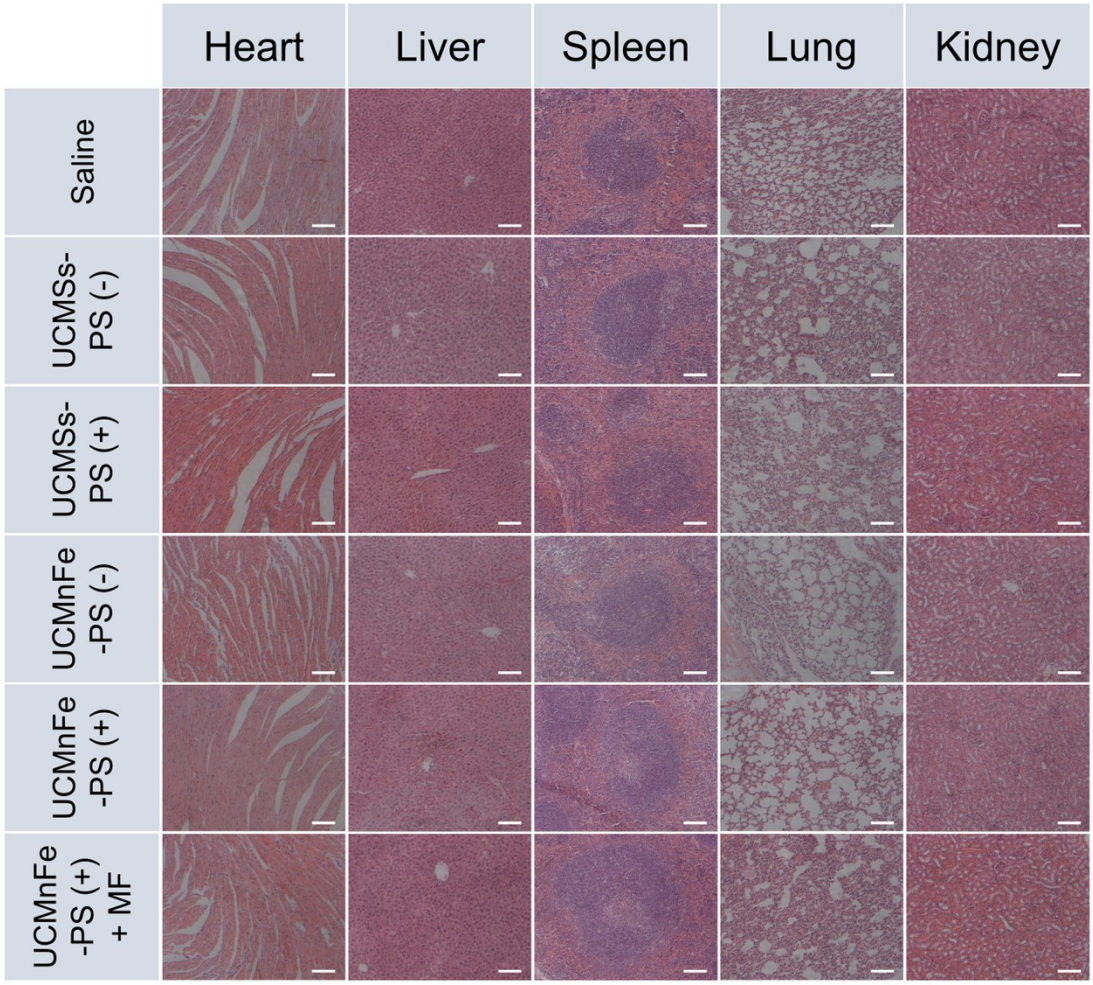

Figure S28. Hematoxylin and eosin (H&E)-stained images of major organs of nude mice after various treatments. All scale bars are 100 μm.

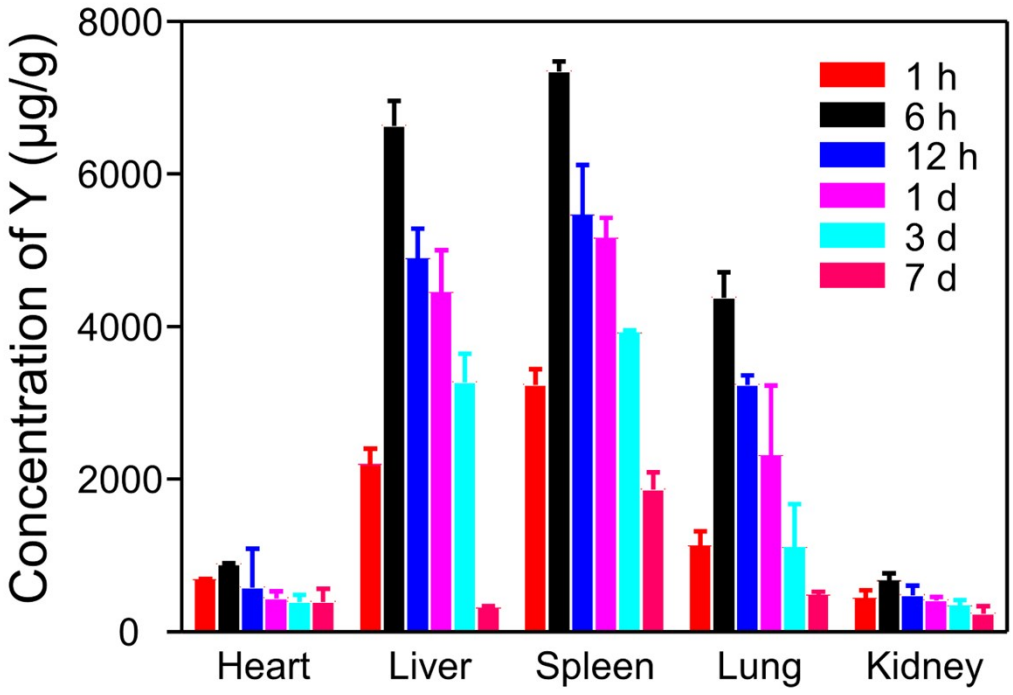

Figure S29. Biodistribution of UCMnFe in mice at different time points (1 h, 6 h, 12 h, 1 days, 3 days and 7 days) post injection measured by ICP-AES (Y levels).

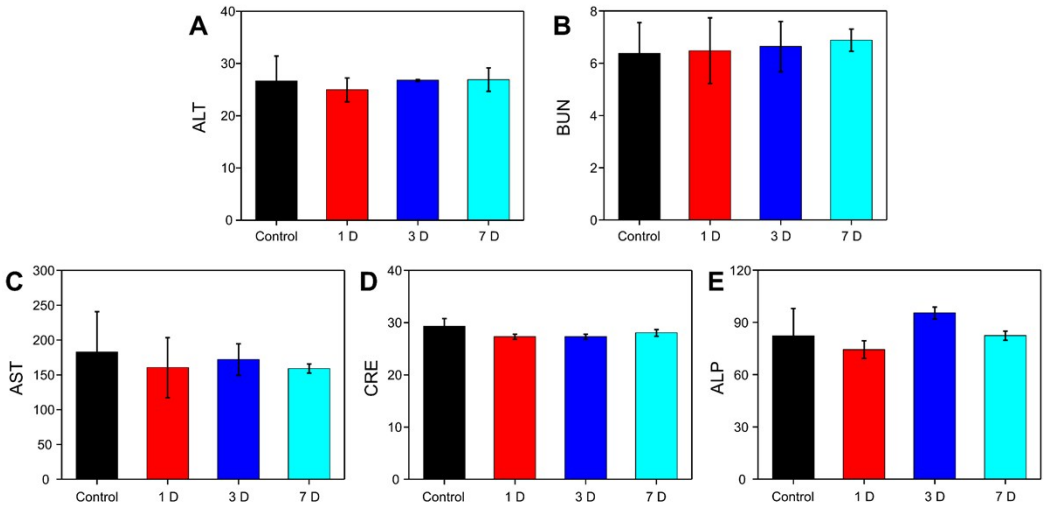

Figure S30. (A-E). Serum biochemistry data including alanine aminotransferase (ALT), blood urea nitrogen (BUN), aspartate aminotransferase (AST), creatinine (CRE), and alkaline phosphatase (ALP).